Characterization of the Walker A Motif of MsbA Using Site-Directed Spin Labeling Electron Paramagnetic Resonance Spectroscopy†

Adam H. Buchaklian and Candice S. Klug*

Department of Biophysics, Medical College of Wisconsin, 8701 Watertown Plank Road, Milwaukee, Wisconsin 53226

Received November 18, 2004; Revised Manuscript Received February 4, 2005

ABSTRACT: MsbA is an ABC transporter that transports lipid A across the inner membrane of Gram-negative bacteria such as *Escherichia coli*. Without functional MsbA present, bacterial cells accumulate a toxic amount of lipid A within their inner membranes. A crystal structure of MsbA was recently obtained that provides an excellent starting point for functional dynamics studies in membranes [Chang and Roth (2001) *Science 293*, 1793−1800]. Although a structure of MsbA is now available, several functionally important motifs common to ABC transporters are unresolved in the crystal structure. The Walker A domain, one of the ABC transporter consensus motifs that is directly involved in ATP binding, is located within a large unresolved region of the MsbA ATPase domain. Site-directed spin labeling (SDSL) electron paramagnetic resonance (EPR) spectroscopy is a powerful technique for characterizing local areas within a large protein structure in addition to detecting and following changes in local structure due to dynamic interactions. MsbA reconstituted into lipid membranes has been evaluated by EPR spectroscopy, and it has been determined that the Walker A domain forms an α-helical structure, which is consistent with the structure of this motif observed in other crystallized ABC transporters. In addition, the interaction of the Walker A residues with ATP before, during, and after hydrolysis was followed using SDSL EPR spectroscopy in order to identify the residues directly involved in substrate binding and hydrolysis.

Multidrug resistance (MDR) is becoming an increasingly serious problem in a number of areas of medicine, especially in the treatment of infectious diseases and cancer (*1*−*7*). ATP binding cassette (ABC) transporters contribute to drug resistance by using ATP hydrolysis to export delivered drugs back across the cell membrane. In addition, serious genetic disorders such as cystic fibrosis (*8*) also result from the function or dysfunction of ABC transporters. The ability of these transporters not only to transport drugs or phospholipids but also to flip them 180° has given rise to names such as flippases and hydrophobic vacuum cleaners (e.g., ref *9*). MDR transporters typically are comprised of two membrane spanning domains and two intracellular ATP binding domains (or nucleotide binding domains, NBDs). Either the entire protein complex is located all on one gene [e.g., human MDR1 (*10*) and the cystic fibrosis transmembrane conductance regulator (CFTR) (*8*)] or two protein monomers form a functional homodimer [e.g., MsbA (*9*, *11*), Rad50 (*12*)]. To better understand the MDR transporters, several crystal structures of various ATP binding cassette transporters (ABC transporters) have been solved and include MsbA (*9*, *11*), MalK (*13*), Rad50 (*12*), and HisP (*14*). These structures reveal that the ATP binding domains typically form the dimer interface, that each NBD binds one ATP molecule, and the transmembrane domains are either attached as six-helix bundles [as in MsbA (*9*, *11*), P-glycoprotein (*15*), and Rad50 (*12*)] or are contained in tightly bound separate proteins such as is the case with the $MalFGK_2$ (*16*) and histidine permease (*17*) complexes. In all cases so far, the dimer form of the protein is necessary for activity, indicating that cooperativity between the two subunits is essential.

MsbA is a 65 kDa ATPase lipid A transporter and is found in the inner membranes of Gram-negative bacteria such as *Escherichia coli* (*18*). Since lipid A is the major component of the outer leaflet of the outer membrane of Gram-negative bacteria, its synthesis and transport are also essential for cell growth. Functional loss of MsbA from the bacterium results in a toxic accumulation of lipid A within the inner membrane (*19*), and it is the only bacterial ABC transporter that is required for bacterial viability (*20*).

A crystal structure of the *E. coli* MsbA homodimer was recently solved to a resolution of 4.5 Å (*9*). The structure reveals that the MsbA monomer contains a transmembrane six-helix bundle linked to a globular nucleotide binding domain (NBD), where ATP is hydrolyzed to provide energy for transport of lipid A. ABC transporters share at least three specifically conserved regions that identify them as ATPases: Walker A and Walker B sequences and an ATP binding consensus sequence that contains the ABC transporter signature sequence LSGGQ. MsbA contains all three of these conserved primary sequences (*18*), and this identified it as an ABC transporter even before the crystal structure confirmed its identity. Interestingly, the segment of MsbA that contains the Walker A sequence was not resolved in the crystal structure (343−419), indicating that it may have potential functional significance due to its apparent flexibility.

Site-directed spin labeling (SDSL)[1] electron paramagnetic resonance (EPR) spectroscopy is a powerful technique that can provide a great deal of information on the location and

† This work was supported by Grant GM070642 from the NIH.

* To whom correspondence should be addressed. Phone: 414-456-4015. Fax: 414-456-6512. E-mail: candice@mcw.edu.

10.1021/bi047568v CCC: $30.25
Published on Web 03/12/2005

environment of an individual residue within a very large and complex protein structure (*21*−*25*). Unlike other methods that allow only the monitoring of global changes in protein structure, SDSL allows the direct probing of the local environment, structure, and proximity of individual residues. Since EPR is not limited by either macromolecular size or the optical properties of the sample, it is especially amenable to the investigation of membrane proteins, as they are normally difficult to study by other spectroscopic methods and are an important and large class of biologically relevant structures. The EPR spectroscopy technique has the unique ability to address and answer questions not solvable by genetic or crystal structure analysis and is especially amenable to the study of the unresolved regions of the MsbA NBD. The studies described here directly address the local structure of the Walker A motif in MsbA and the effect of ATP binding on the conformation of this domain.

EXPERIMENTAL PROCEDURES

Materials

Lipids were purchased from Avanti Polar Lipids (Alabaster, AL), the nitroxide spin label MTSL (2,2,5,5-tetramethylpyrrolin-3-ylmethanethiosulfonate spin label) was purchased from Toronto Research Chemicals (Ontario, Canada), and dodecyl maltoside (DM) was obtained from Alexis Biochemicals (San Diego, CA).

Methods

Site-Directed Mutagenesis and Protein Purification. The gene encoding the *E. coli* MsbA protein was obtained and inserted into a pET28b vector (Novagen) with an N-terminal 6×His tag as previously described (*26*). In addition, both native cysteines (C88 and C315) were previously substituted with serines to create a cysteine-less construct (*26*). Single cysteines at positions 378−390 were individually introduced into the cysteine-less MsbA plasmid by site-directed mutagenesis using the QuikChange mutagenesis kit (Stratagene). Mutant plasmids were sequenced by the MCW Protein and Nucleic Acid Facility (Milwaukee, WI) for verification of the introduced cysteine mutation. The plasmids containing the MsbA gene mutations were transformed into NovaBlue cells (Novagen), and the 6×His-tagged MsbA protein was purified by cobalt affinity chromatography using Talon resin (BD Biosciences Clontech) as described previously (*26*). MsbA G379C was found to be disulfide bonded with itself upon purification and was not successfully used in the EPR experiments due to extremely low labeling efficiencies, even after being subjected to reducing agents.

Activity Assays. ATPase activity of the cysteine-less MsbA construct was previously determined to be similar to that of WT MsbA (*26*). All newly introduced cysteine mutants in the cysteine-less background were assayed for ATPase activity in the presence and absence of lipid A using a colorimetric assay to detect the release of P_i following ATP hydrolysis (*27*). Briefly, the basal level of ATPase activity in each MsbA mutant in detergent micelles was measured followed by activity measurements due to lipid A stimulation. All cysteine mutants were able to hydrolyze ATP and showed on average a 25−50% increase in ATPase activity upon the addition of lipid A. In addition, activities for each of the spin-labeled proteins were similar to unlabeled protein with the exception of sites 380, 382, and 386, which although they have good basal activity are not stimulated by lipid A.

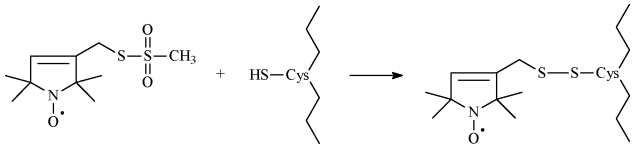

FIGURE 1: The sulfhydryl-specific spin label MTSL reacts directly with the introduced cysteine residue to form a covalent disulfide bond between the protein and the spin label.

Sample Preparation. MsbA cysteine mutants were labeled with a 10:1 molar ratio of the sulfhydryl-specific spin label 2,2,5,5-tetramethylpyrrolin-3-ylmethanethiosulfonate spin label (MTSL; Figure 1) overnight at 4 °C in 50 mM sodium phosphate, 0.01% DM, pH 7.0, buffer. Excess label was removed by extensive dialysis against 50 mM sodium phosphate, 0.01% DM, pH 7.0, buffer, and protein concentrations were determined by a detergent-compatible BCA protein assay (Pierce) using BSA as a protein standard. The major phospholipids of the inner membrane of *E. coli* are phosphatidylethanolamine (PE), phosphotidylglycerol (PG), and cardiolipin (CL). These purified lipids were purchased in chloroform and mixed at a molar ratio of 65:25:10 PE:PG:CL, dried down under nitrogen, desiccated, and then resuspended and solubilized in DM prior to the addition of MsbA at a protein:lipid molar ratio of 1:500. Bio-Beads (Bio-Rad) were added to the mixture in order to remove the detergent, and the resulting proteoliposome solution was then concentrated by high-speed centrifugation (30 min at 100000*g*). The proteoliposomes were resuspended in the appropriate volume of phosphate buffer, or phosphate buffer containing NiEDDA, and freeze−thawed four times to allow complete equilibration of the NiEDDA to both sides of the bilayer. Proteolipid samples containing substrate typically had final concentrations of 100 μM protein, 40 mM ATP, 2 mM EDTA, 40 mM $MgCl_2$, and 2 mM sodium orthovanadate (V_i), similar to those previously described for the maltose transporter (*28*).

Electron Paramagnetic Resonance Spectroscopy. Continuous wave (CW) EPR spectroscopy was carried out at X-band on a Bruker ELEXSYS E500 fitted with a super high Q (SHQ) cavity, and power saturation measurements were carried out on a Varian E-102 Century series spectrometer equipped with a loop-gap resonator (Medical Advances, Milwaukee, WI). Samples were contained in either a glass capillary or a gas-permeable TPX capillary for gas equilibration during accessibility measurements. Saturation data were collected and analyzed using LabView data collection and analysis programs written by Christian Altenbach (UCLA).

The accessibility of a spin label to paramagnetic reagents decreases the effective spin−lattice relaxation time, T_1, which results in an increase in the measured power saturation ($P_{1/2}$) value. Thus, the more accessible a spin label is to a given

[1] Abbreviations: SDSL, site-directed spin labeling; EPR, electron paramagnetic resonance; CW, continuous wave; NiEDDA, nickel ethylenediaminediacetic acid; LGR, loop-gap resonator; MTSL, methanethiosulfonate spin label; DM, dodecyl maltopyranoside; PE, phosphatidylethanolamine; PG, phosphatidylglycerol; CL, cardiolipin; SDS−PAGE, sodium dodecyl sulfate−polyacrylamide gel electrophoresis; DTT, dithiothreitol.

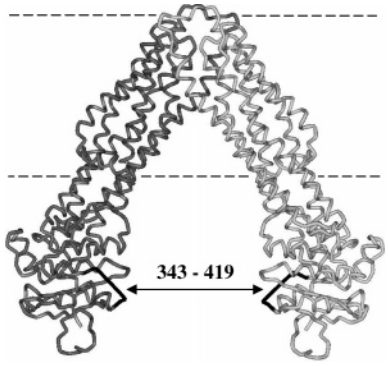

FIGURE 2: The crystal structure of the *E. coli* MsbA homodimer (*9*) is shown with the unresolved 75 amino acid region highlighted. The Walker A motif is located within this unresolved region of the NBD. The location of the membrane interface based on previous data is indicated by the dashed lines (*26*).

paramagnetic reagent, the higher the $P_{1/2}$ value since the power required for saturation is increased due to collisions of the spin label with the paramagnetic relaxation reagent. Therefore, the change in $P_{1/2}$ relative to a standard measured under N_2 [e.g., $P_{1/2}(O_2) - P_{1/2}(N_2) = \Delta P_{1/2}(O_2)$] is directly proportional to the bimolecular collision rate of the spin label with the paramagnetic probe (*29*). The TPX capillary was equilibrated with a stream of either nitrogen or air (20% oxygen) during the power saturation experiments. The $P_{1/2}$ values for each sample in the presence of nitrogen, air, or 175 mM NiEDDA under nitrogen were recorded and calculated as described by Altenbach et al. (*30*). $\Delta P_{1/2}$ values were determined by subtracting the nitrogen $P_{1/2}$ values from each of the air and NiEDDA $P_{1/2}$ parameters, and the Π values were calculated to account for line width variation as previously described (*31*).

RESULTS

The crystallographic configuration of the *E. coli* MsbA homodimer is shown in Figure 2 with the dotted lines indicating its placement within a membrane bilayer (*26*). A large region in the NBD was unresolved in the crystal structure and is indicated by a straight black line in the figure to account for the structural gap between residues 343 and 419 in each monomer. The Walker A consensus sequence for MsbA is contained within this region, spanning residues 378−390.

Resting State Accessibility Data. CW power saturation EPR spectroscopy has proven to be a convenient method for determining the local environment of introduced spin label side chains within a large protein structure. This is an especially useful technique for determining local secondary structure of unresolved regions of a protein and is clearly applicable to the study of the unresolved Walker A motif in MsbA. Each of the residues in the Walker A domain of MsbA, 378−390, were individually analyzed for their accessibilities to the paramagnetic broadening reagents oxygen and NiEDDA. The results obtained from the power saturation measurements are plotted in Figure 3. Residues 378−381 show no sign of secondary structure, which is indicative of a loop region, whereas a curve with a periodicity of 3.6 is apparent for residues 382−390, indicating clear α-helical structure in this region. Although the higher accessibility of site 389 to oxygen causes a dampening of

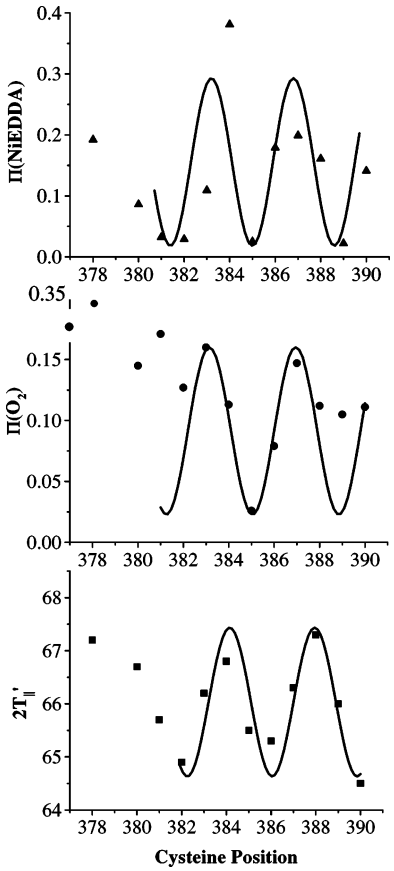

FIGURE 3: Accessibility plots of the Walker A motif in MsbA. CW EPR power saturation results are shown for each residue from 378 to 390 in the presence of air (20% oxygen) and 20 mM NiEDDA. Accessibility to each paramagnetic reagent increases with increasing Π values. The outer hyperfine splittings ($2T_{||}'$) for each of the sites are also plotted versus position. Sine curves with a periodicity of 3.6 are overlaid onto the data.

the amplitude of the oxygen periodicity near the end of this helix and the increased accessibility of 384 to NiEDDA results in an increased amplitude in periodicity, the 3.6 residue periodicity remains constant throughout the nearly three turns of the helix. Due to the larger size of NiEDDA compared to molecular oxygen, NiEDDA is a better discriminator of secondary structure in extramembranous helices than oxygen, which may account for the differences in accessibility observed at position 389 in the last turn of the helix. Although the outer splittings for each spectrum ($2T_{||}'$) report only on the most immobile spectral components, these values can be useful for secondary structure prediction and therefore are plotted as a function of position in Figure 3. These data clearly verify the helical periodicity predicted from the accessibility data collected from the center lines. The in-phase periodicity observed for oxygen and NiEDDA accessibilities is expected for a soluble protein domain such as the MsbA NBD, as opposed to a membrane exposed domain where the accessibilities are expected to be out of phase with respect to each other. In solution, the side chains are accessible to both oxygen and NiEDDA, revealing an in-phase periodicity, whereas there is an inverse concentration gradient of oxygen and NiEDDA within membrane bilayers that results in an out-of-phase periodicity of the accessibilities.

The power saturation results are in excellent agreement with the crystal structures of the Walker A domains from

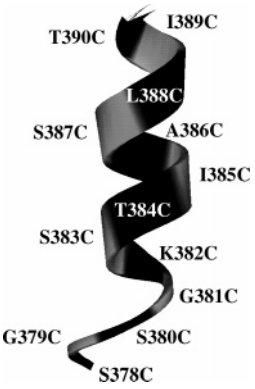

FIGURE 4: Cartoon of the secondary structure of the *E. coli* MsbA Walker A domain based on the EPR results presented here. Sites 378−390 are labeled at their respective positions in the structure, with odd-numbered residues indicated in gray. A similar structure is also observed for the *V. cholera* MsbA (*11*) and *E. coli* MalK (*13*) Walker A domains.

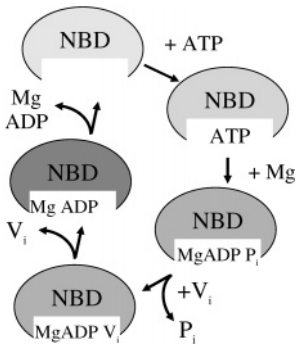

FIGURE 5: ATP binding and hydrolysis. Each monomer of MsbA contains an ATP binding site, as illustrated in cartoon form. The four stages of hydrolysis are shown where ATP binds and is hydrolyzed to ADP and P_i upon the addition of $MgCl_2$, followed by dissociation of the P_i and finally by the dissociation of ADP to return to the resting state.

both *Vibrio cholera* MsbA (*11*) and *E. coli* MalK (*13*) where the corresponding residues 378−382 form a loop structure preceding an α-helix containing the residues corresponding to positions 383−390 (Figure 4). In addition, sequence homology comparison to other ATP binding proteins, such as the MJ0796 dimer (*32*), reveals that sites corresponding to MsbA 382−390 also form an α-helix within the Walker A motif, consistent with our results for MsbA.

Substrate Binding. To observe the changes occurring during ATP hydrolysis in MsbA, the EPR spectra were recorded at four different stages of this pathway. Figure 5 illustrates in cartoon form the four different steps considered for each monomer in the ATP hydrolysis studies. The resting state of each spin-labeled protein was recorded in the absence of any substrate. Next, the ATP-bound, prehydrolysis state was trapped by the addition of EDTA in order to chelate any magnesium ions that may be present, which are required for cleavage of the ATP γ-phosphate during hydrolysis. Nonhydrolyzable ATP analogues such as AMP-PNP can also be used to trap this intermediate state. To trap the high-energy intermediate immediately following hydrolysis, both ATP and magnesium were added to the ATPase directly followed by vanadate. The addition of vanadate to replace the hydrolyzed phosphate resulted in the inability of ADP and vanadate to be released from the binding pocket, allowing for the analysis of this transition state over an extended period of time. Finally, the posthydrolysis ADP-bound state was induced by the addition of excess ATP and magnesium, allowing the hydrolysis reaction to proceed.

First, the spectra of each spin-labeled mutant from sites 378−390 were recorded in the resting state after reconstitution into lipid bilayers (Figure 6). Each spin-labeled site resulted in a spectrum with at least two motional components (see Figure 7). Each site shows the presence of one fairly immobile component and a smaller proportion of a more mobile component. In the case of 378 and 380, the spectra indicate a larger population of the faster motional component than the remaining spectra, whereas 384 appears to contain three motional components, and 385 is largely immobilized in the resting state.

Next, an excess of ATP and EDTA were added to each sample in order to generate the ATP-bound state prior to hydrolysis. Changes in the motional components of many of the spectra examined were observed. Some of the changes observed were shifts in the equilibrium between the two motional states, such as large changes in 378 (Figure 7A) and 384 and a subtle change in 387, where they all shifted toward the more immobile conformation. As an example, Figure 7A shows the overlay of the resting state 378 spectrum and the ATP-bound spectrum to illustrate the shift in motional populations. In some cases, as with 378, this shift is very evident, while in cases such as 387, this shift is subtle and is more apparent upon direct overlay of the spectra. As some spectra shifted the equilibrium between their motional states, others became much more immobile as evidenced by an outward shift in the spectral breadth of the outer lines. Sites 380, 382, and 385 showed significant changes in motion, all becoming even more immobilized in the ATP-bound state. With the exception of 389, the most significant changes occurred at residues 378−385. These changes are consistent with the literature for crystallized ATP-bound ATPases (e.g., refs *32* and *33*) where the 378−384 side chains have been shown to be directly involved in binding to the ATP molecule.

The transition state immediately following hydrolysis was induced by the addition of excess ATP and magnesium to produce ADP and P_i and was followed by the rapid replacement of the cleaved P_i with vanadate, forming a stable transition state complex. Sites 378 through 385 all had considerable motional changes upon ATP hydrolysis, as seen in the EPR spectra (Figure 6). Each of these residues showed a shift toward their more restricted component. In addition, the outer peaks of 382 and 385 also moved outward, indicating even slower motion in the more restricted populations at these sites. Figure 7B illustrates the clear increase in the more immobile population for site 378 upon vanadate trapping coupled with a marked decrease in the mobile population. Residues 386−390 did not show any further changes in this transition state from the ATP-bound state. These results suggest that a conformational change occurs in the entire 378−385 Walker A region upon hydrolysis of ATP, whereas 386−390 are unaffected at this step.

The final state examined was the posthydrolysis ADP-bound state, generated by the addition of excess ATP and magnesium. A shift in the motional components of 378 (Figure 7C), 380, 382, and 383 was observed where they each showed an increase in their more mobile states, and 384 also has a similar but less evident change, whereas 385

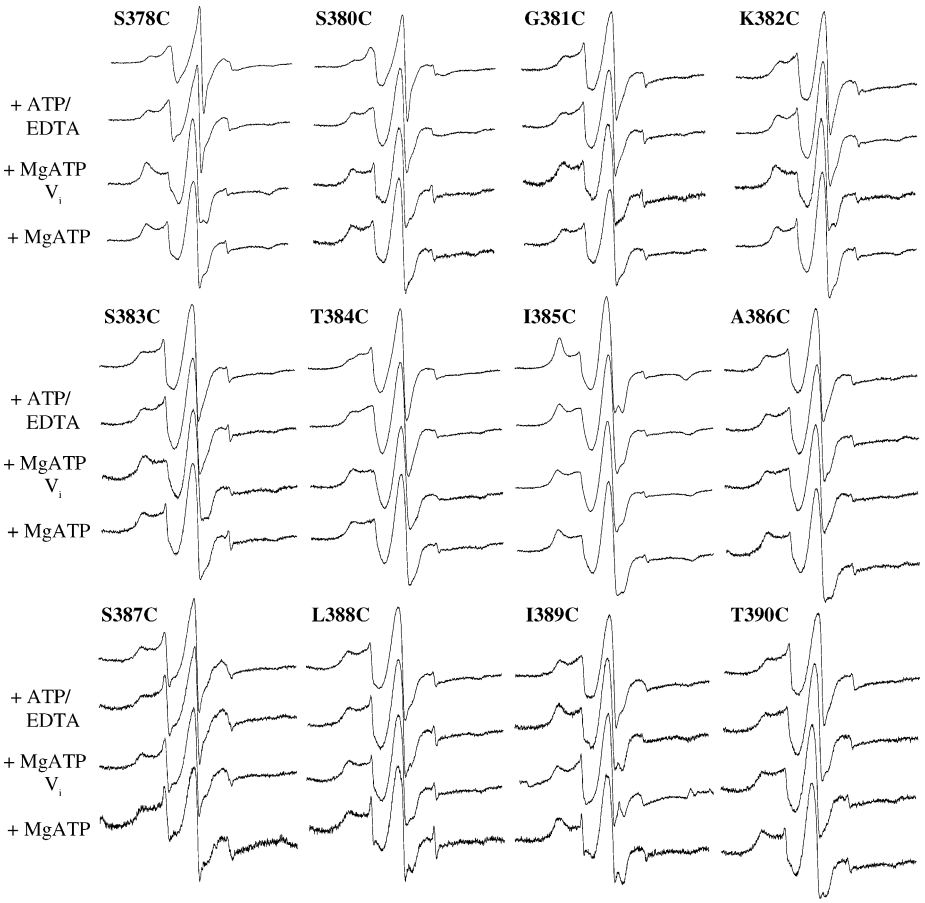

FIGURE 6: CW X-band EPR spectra of each MTSL-labeled MsbA mutant reconstituted into inner membrane liposomes from 378 to 390 are shown for each step in ATP hydrolysis. Spectra were recorded at room temperature with a 100 G scan width, 10 mW microwave power, and 36−49 signal averages with a typical protein concentration of 100 μM. Spectra in the resting state (no substrate) are shown as the top spectrum in each series, with the addition of substrate as indicated in the margin.

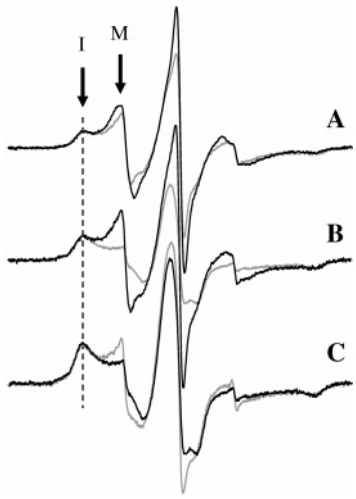

FIGURE 7: Spectral overlays of spin-labeled MsbA S378C. (A) The resting state spectrum of 378 (black) and the ATP-bound spectrum (gray) are shown overlaid to illustrate the motional changes observed in the spectra upon addition of substrate. (B) The ATP-bound (black) and the vanadate-trapped (gray) spectra are overlaid to show the shift in motional populations. (C) The vanadate-trapped spectrum (black) and the ADP-bound spectrum (gray) are shown as overlays. All spectra are aligned by the intensity of the low-field immobilized component (I arrow and dashed line). The M arrow indicates the more mobile motional components of the spectra.

and 386 actually showed an increase in their more restricted motional components. Sites 387−389 showed no change from the posthydrolysis transition state, while 390 also showed a slight increase in its more immobile population. In all cases, the changes observed at sites 378−385 upon ATP binding and hydrolysis are consistent with these being the relevant Walker A residues involved in substrate binding.

In the experiments containing all of the components necessary for hydrolysis to proceed, we assumed that the posthydrolysis ADP-bound state is represented; however, it is also possible that the relaxed transporter with ADP rebound was observed. To determine if there was a difference between these two ADP-bound states, the spectra from 378 to 385 were recorded with excess ADP added to the samples. The resulting spectra were all very similar to the posthydrolysis spectra and were motionally different from the resting state spectra. These results indicate that the transporter relaxes once the P_i is released from the binding site and that there is no significant difference between the posthydrolysis ADP-bound state and ADP binding directly to the relaxed transporter. However, the ADP-bound state observed in both cases in the studies presented here is distinct from the resting and ATP-bound states for sites 378−385.

To follow overall conformational changes in this region during hydrolysis, the vanadate-trapped transition state was examined by power saturation methods and compared to the resting state conformation determined earlier. Only those residues shown to undergo conformational changes upon vanadate trapping of the high-energy transition state (378−385) were monitored for accessibility. As before, each of

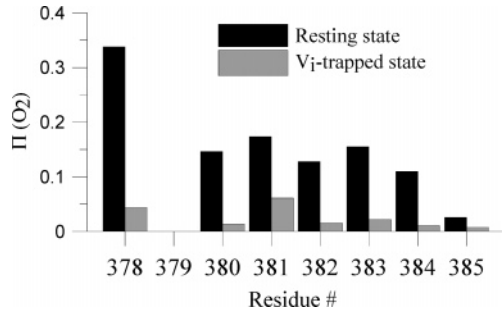

FIGURE 8: Oxygen accessibility comparison for Walker A sites 378−385. The black bars indicate the resting state accessibilities to 20% oxygen (air), and the gray bars indicate the oxygen accessibilities in the vanadate-trapped transition state.

the residues from 378 to 385 was analyzed for their accessibilities to the paramagnetic broadening reagents oxygen and NiEDDA. The results obtained from the power saturation measurements in the transition state for this region followed the same secondary structure observed for the resting state; however, a significant decrease in accessibility was observed for each of these sites in going from the resting state to the vanadate-trapped transition state. Figure 8 specifically compares the decrease in the oxygen accessibilities between the resting and vanadate-trapped states. These results indicate that the overall secondary structure of this region remains intact during hydrolysis, although considerable changes in the dynamics of many of the side chains occur.

DISCUSSION

The studies described here directly identify the local secondary structure of the Walker A motif in *E. coli* MsbA and the effects on the local conformational dynamics of each position during ATP binding and hydrolysis. This motif is comprised of a loop region followed by an α-helix in both the resting and activated states. In addition, conformational changes are observed in the 378−385 region upon ATP binding and hydrolysis, directly identifying which residues are involved in the functional dynamics of substrate binding and turnover, and our results are in agreement with the residues predicted to be involved in substrate binding based on crystallized ATP-bound structures of other ATPases (e.g., refs *13* and *32*).

All of the resting state spectra recorded contained at least two motional components. More than one motional component in a spectrum can be derived either from two different rotameric states of the spin label side chain or from two different configurations of the MsbA homodimer, which would be indicative of an equilibrium between two different conformational states of MsbA. Both of these scenarios are possible in this case; however, it is more likely that there are two different conformations of the spin label side chain and that the equilibrium is shifted in the rotameric state of the side chain, indicating local conformational changes within the protein upon ligand binding and hydrolysis.

Upon ATP binding, residues 378, 380, 382, and 384 became more restricted in their motion due to the presence of ATP; however, the motion of site I385C became more mobile. This indicates that site 385 is likely normally motionally restricted due to packing with neighboring side chains, but upon ATP binding, the movement of the entire helix or changes in the positions of the neighboring side chains allow for more motional flexibility at this site. Interestingly, sites G381C and S383C did not show any spectral changes upon binding of ATP. This could be due to their side chains being oriented on the opposite side of the helix from the ATP binding site. Previous studies indicate that either the protein backbone or the side chains themselves of sites 378−384 are involved in binding directly to ATP (*32*, *33*). It is possible that although these two sites do directly interact with ATP, the motional states of the spin label side chain are not perturbed. Activity studies for these cysteine-substituted proteins show that they do in fact hydrolyze ATP and both of these sites are affected in later steps of hydrolysis. It was expected that ATP binding would affect residues 378−385; however, the changes observed at S387C and I389C were slightly unexpected and are probably due to structural rearrangements around the helix upon ATP binding.

In addition to using ATP in the presence of EDTA to chelate any magnesium ions in the sample to prevent hydrolysis from occurring before the spectrum was recorded, the nonhydrolyzable ATP analogue, AMP-PNP, was also used in several of the 378−385 experiments (data not shown). The spectrum of one of the proteins (K382C) in the presence of AMP-PNP was the same as its spectrum in the presence of ATP/EDTA, while the spectra of the remaining proteins tested were shifted back toward those found in their resting state (S378C, S380C, I385C). The ATP/EDTA sample lacks a bound magnesium in the binding pocket, but since ATP is the native substrate, a possibility exists to continue through hydrolysis, while the AMP-PNP sample contains a non-native substrate analogue and is absolutely unable to continue through hydrolysis. The lack of magnesium in the ATP samples could account for the changes in mobility at some of these sites; however, it is also possible that the ATP analogue does not induce quite the same structural changes as the native ATP. Another commonly used ATP analogue, ATPγS, was not used in these experiments as the sulfur was previously shown to remove the spin label from the protein, resulting in an additional unwanted spectral component (*28*).

Despite the high sequence homology between the *E. coli* and *V. cholera* MsbA proteins, the crystal structures vary significantly. Not only are the helical bundles of the *V. cholera* structure in a more closed conformation within the homodimer but the NBDs are notably rearranged, with functionally important domains such as the Walker A motif in very different locations within each NBD and with respect to each other within the homodimer. Unlike the *E. coli* protein studied here, the secondary structure of the Walker A motif was resolved in the *V. cholera* structure, and the EPR data align extremely well with the secondary structure found in the *V. cholera* crystal, despite global structural differences between the crystal structures of the NBDs in the two proteins.

In summary, our studies indicate that the Walker A domain in the reconstituted *E. coli* MsbA protein is comprised of the same loop−helix secondary structural motif found in previously crystallized ATPases. Residues in the region of 378−385 undergo significant side chain rearrangements upon ATP binding and hydrolysis, yet the secondary structural elements remain intact.

ACKNOWLEDGMENT

We thank Andrea Funk, Megan Morrell, Kyle Bantz, and Nick Kettenhofen for assistance on this project and Jimmy Feix for critical reading of the manuscript.

REFERENCES

1. Poole, K. (2003) Overcoming multidrug resistance in gram-negative bacteria, *Curr. Opin. Invest. Drugs 4*, 128−139.
2. Leonessa, F., and Clarke, R. (2003) ATP binding cassette transporters and drug resistance in breast cancer, *Endocr. Relat. Cancer 10*, 43−73.
3. Nachega, J. B., and Chaisson, R. E. (2003) Tuberculosis drug resistance: a global threat, *Clin. Infect. Dis. 36*, S24−S30.
4. Thomas, H., and Coley, H. M. (2003) Overcoming multidrug resistance in cancer: an update on the clinical strategy of inhibiting p-glycoprotein, *Cancer Control 10*, 159−165.
5. Tsuruo, T., Naito, M., Tomida, A., Fujita, N., Mashima, T., Sakamoto, H., and, Haga, N. (2003) Molecular targeting therapy of cancer: drug resistance, apoptosis and survival signal, *Cancer Sci. 94*, 15−21.
6. Kellen, J. A. (2003) The reversal of multidrug resistance: an update, *J. Exp. Ther. Oncol. 3*, 5−13.
7. Gottesman, M. M., and Ambudkar, S. V. (2001) Overview: ABC transporters and human disease, *J. Bioenerg. Biomembr. 33*, 453−458.
8. Cotten, J. F., and Welsh, M. J. (1997) Covalent modification of the regulatory domain irreversibly stimulates cystic fibrosis transmembrane conductance regulator, *J. Biol. Chem. 272*, 25617−25622.
9. Chang, G., and Roth, C. B. (2001) Structure of MsbA from *E. coli*: a homolog of the multidrug resistance ATP binding cassette (ABC) transporters, *Science 293*, 1793−1800.
10. Chen, C. J., Clark, D., Ueda, K., Pastan, I., Gottesman, M. M., and Roninson, I. B. (1990) Genomic organization of the human multidrug resistance (MDR1) gene and origin of P-glycoproteins, *J. Biol. Chem. 265*, 506−514.
11. Chang, G. (2003) Structure of MsbA from *Vibrio cholera*: a multidrug resistance ABC transporter homolog in a closed conformation, *J. Mol. Biol. 330*, 419−430.
12. Hopfner, K. P., Karcher, A., Shin, D. S., Craig, L., Arthur, L. M., Carney, J. P., and Tainer, J. A. (2000) Structural biology of Rad50 ATPase: ATP-driven conformational control in DNA double-strand break repair and the ABC-ATPase superfamily, *Cell 101*, 789−800.
13. Diederichs, K., Diez, J., Greller, G., Muller, C., Breed, J., Schnell, C., Vonrhein, C., Boos, W., and Welte, W. (2000) Crystal structure of MalK, the ATPase subunit of the trehalose/maltose ABC transporter of the archaeon *Thermococcus litoralis*, *EMBO J. 19*, 5951−5961.
14. Hung, L. W., Wang, I. X., Nikaido, K., Liu, P. Q., Ames, G. F., and Kim, S. H. (1998) Crystal structure of the ATP-binding subunit of an ABC transporter, *Nature 396*, 703−707.
15. Rosenberg, M. F., Kamis, A. B., Callaghan, R., Higgins, C. F., and Ford, R. C. (2003) Three-dimensional structures of the mammalian multidrug resistance P-glycoprotein demonstrate major conformational changes in the transmembrane domains upon nucleotide binding, *J. Biol. Chem. 278*, 8294−8299.
16. Fetsch, E. E., and Davidson, A. L. (2003) Maltose transport through the inner membrane of *E. coli*, *Front. Biosci. 8*, D652−D660.
17. Ames, G. F., Nikaido, K., Wang, I. X., Liu, P. Q., Liu, C. E., and Hu, C. (2001) Purification and characterization of the membrane-bound complex of an ABC transporter, the histidine permease, *J. Bioenerg. Biomembr. 33*, 79−92.
18. Karow, M., and Georgopoulos, C. (1993) The essential *Escherichia coli* msbA gene, a multicopy suppressor of null mutations in the htrB gene, is related to the universally conserved family of ATP-dependent translocators, *Mol. Microbiol. 7*, 69−79.
19. Zhou, Z., White, K. A., Polissi, A., Georgopoulos, C., and Raetz, C. R. (1998) Function of *Escherichia coli* MsbA, an essential ABC family transporter, in lipid A and phospholipid biosynthesis, *J. Biol. Chem. 273*, 12466−12475.
20. Karow, M., and Georgopoulos, C. (1993) The essential *Escherichia coli* msbA gene, a multicopy suppressor of null mutations in the htrB gene, is related to the universally conserved family of ATP-dependent translocators, *Mol. Microbiol. 7*, 69−79.
21. Klug, C. S., and Feix, J. B. (2004) SDSL: A survey of biological applications, in *Biological Magnetic Resonance* (Berliner, L. J., Eaton, S. S., and Eaton, G. R., Eds.) Vol. 24, pp 269−308, Kluwer Academic/Plenum Publishers, Hingham, MA.
22. Klug, C. S., Su, W., and Feix, J. B. (1997) Mapping of the residues involved in a proposed beta-strand located in the ferric enterobactin receptor FepA using site-directed spin-labeling, *Biochemistry 36*, 13027−13033.
23. Hubbell, W. L., Cafiso, D. S., and Altenbach, C. (2000) Identifying conformational changes with site-directed spin labeling, *Nat. Struct. Biol. 7*, 735−739.
24. Hubbell, W. L., Gross, A., Langen, R., and Lietzow, M. A. (1998) Recent advances in site-directed spin labeling of proteins, *Curr. Opin. Struct. Biol. 8*, 649−656.
25. Isas, J. M., Langen, R., Haigler, H. T., and Hubbell, W. L. (2002) Structure and dynamics of a helical hairpin and loop region in annexin 12: a site-directed spin labeling study, *Biochemistry 41*, 1464−1473.
26. Buchaklian, A. H., Funk, A. L., and Klug, C. S. (2004) Resting state conformation of the MsbA homodimer as studied by site-directed spin labeling, *Biochemistry 43*, 8600−8606.
27. Gonzalez-Romo, P., Sanchez-Nieto, S., and Gavilanes-Ruiz, M. (1992) A modified colorimetric method for the determination of orthophosphate in the presence of high ATP concentrations, *Anal. Biochem. 200*, 235−238.
28. Austermuhle, M. I., Hall, J. A., Klug, C. S., and Davidson, A. L. (2004) Maltose-binding protein is open in the catalytic transition state for ATP hydrolysis during maltose transport, *J. Biol. Chem. 279*, 28243−28250.
29. Altenbach, C., Flitsch, S. L., Khorana, H. G., and Hubbell, W. L. (1989) Structural studies on transmembrane proteins. 2. Spin labeling of bacteriorhodopsin mutants at unique cysteines, *Biochemistry 28*, 7806−7812.
30. Altenbach, C., Greenhalgh, D. A., Khorana, H. G., and Hubbell, W. L. (1994) A collision gradient method to determine the immersion depth of nitroxides in lipid bilayers: application to spin-labeled mutants of bacteriorhodopsin, *Proc. Natl. Acad. Sci. U.S.A. 91*, 1667−1671.
31. Farahbakhsh, Z. T., Altenbach, C., and Hubbell, W. L. (1992) Spin labeled cysteines as sensors for protein−lipid interaction and conformation in rhodopsin, *Photochem. Photobiol. 56*, 1019−1033.
32. Smith, P. C., Karpowich, N., Millen, L., Moody, J. E., Rosen, J., Thomas, P. J., and Hunt, J. F. (2002) ATP binding to the motor domain from an ABC transporter drives formation of a nucleotide sandwich dimer, *Mol. Cell 10*, 139−149.
33. Chen, J., Lu, G., Lin, J., Davidson, A. L., and Quiocho, F. A. (2003) A tweezers-like motion of the ATP-binding cassette dimer in an ABC transport cycle, *Mol. Cell 12*, 651−661.

BI047568V